Digital Object Identifier:
https://doi.org/10.1109/JPHOTOV.2019.2922323

doi.org/10.1109/JPHOTOV.2019.2922323

Rear Optical Reflection and Passivation Using a Nanopatterned Metal/dielectric Structure in Thin Film Solar Cells

T. S. Lopes[#], J. M. V. Cunha[#,*], S. Bose, J. R. S. Barbosa, J. Borme, O. Donzel-Gargand, C. Rocha, R. Silva, A. Hultqvist, W. C. Chen, A. G. Silva, M. Edoff, P. A. Fernandes and P. M. P. Salomé

Abstract — **Currently, one of the main limitations in ultrathin Cu(In,Ga)Se_2 (CIGS) solar cells are the optical losses, since the absorber layer is thinner than the light optical path. Hence, light management, including rear optical reflection and light trapping is needed. In this work we focus on increasing the rear optical reflection. For this, a novel structure based on having a metal interlayer in between the Mo rear contact and the rear passivation layer is presented. In total, eight different metallic interlayers are compared. For the whole series, the passivation layer is aluminum oxide (Al_2O_3). The interlayers are used to enhance the reflectivity of the rear contact and thereby increasing the amount of light reflected back into the absorber. In order to understand the effects of the interlayer in the solar cell performance both from optical and/or electrical point of view, optical simulations were performed together with fabrication and electrical measurements. Optical simulations results are compared with current density-voltage (J-V) behavior and external quantum efficiency (EQE) measurements. A detailed comparison between all the interlayers is done, in order to identify the material with the greatest potential to be used as rear reflective layer for ultrathin CIGS solar cells and to establish fabrication challenges. The Ti-W alloy is a promising rear reflective layer since it provides solar cells with light to power conversion efficiency values of 9.9 %, which is 2.2 % (abs) higher than the passivated ultrathin sample and 3.7 % (abs) higher than the unpassivated ultrathin reference sample.**

***Index Terms* — Thin film solar cells, optical simulation, light trapping, back/rear contact, Cu(In,Ga)Se_2**

I. Introduction

Cu(In,Ga)Se_2 thin film solar cells currently achieve a light to power conversion efficiency higher than multicrystalline silicon solar cells (23.35 % vs 22.3 %) [1], [2]. Nonetheless, there is still room for further improvements from both fabrication and performance point of view in CIGS solar cells. If CIGS module production continues on the growth rate as indicated by the latest market trends, the continuing cost-reduction might be compromised in the midterm, due to indium scarcity [3]. Thus, decreasing the absorber thickness to the ultrathin range (sub 500 nm absorber thickness) is highly desirable as it allows material consumption reduction, and, at the same time, the production cost of CIGS solar cells, as throughput could increase due to shorter deposition times. If the efficiency values can be kept the same for ultrathin devices as the ones for standard thickness, a thinner CIGS layer, with a production four times faster than existing ones, would allow for significant increase of machine throughput if pumping times are independent. Furthermore, it has been predicted that ultrathin devices have lower values of bulk recombination, opening a path for more efficient devices [4]. However, when going to the ultrathin range, achieving an electrical performance as high as the thick counterparts is extremely challenging, since performance is limited by two factors: i) interface recombination; and ii) incomplete light absorption [5]. Hence, due to the research on ultrathin devices being quite recent, these two problems need to be tackled so that the performance of ultrathin devices can reach competitive values.

Rear interface recombination can be mitigated by the implementation of a dielectric layer at the rear with nanosized point contacts [6]. This strategy was first employed in silicon technology [7]. Aluminum oxide, Al_2O_3, is a dielectric material that found success as a passivation material, firstly, in the silicon technology, and lately incorporated in the CIGS technology [4], [8]–[11]. Despite the advances addressing the rear recombination, optical losses are still a major challenge being studied by the solar cells community on ultrathin devices [12]–[15]. Major optical losses in the infrared region occur mainly due to the ultrathin CIGS thickness being insufficient to fully absorb the incoming light [5]. Moreover, the poor optical reflectivity of the rear contact (Mo) also accounts for the optical losses as it absorbs the long wavelength light that is not absorbed by the CIGS layer [16]. The optimum optical solution would be to replace Mo with materials with higher reflectivity, such as gold (Au), silver (Ag) or copper (Cu). However, these

# Authors contributed equally

* Corresponding author: J. M. V. Cunha (jose.cunha@inl.int).

Fundação para a Ciência e a Tecnologia (FCT) is acknowledged trough: IF/00133/2015 and PD/BD/142780/2018. The European Union's Horizon 2020 research and innovation programme ARCIGS-M project (grant agreement no. 720887) is acknowledged. This research is also supported by NovaCell (028075) and InovSolarCells (029696) co-funded by FCT and the ERDF through COMPETE2020.

T. S. Lopes, J. M. V. Cunha, S. Bose, J. R. S. Barbosa, J. Borme, O. Donzel-Gargand, C. Rocha, R. Silva, P. A. Fernandes and P. M. P. Salomé are with INL – International Iberian Nanotechnology Laboratory, Avenida Mestre José Veiga, 4715-330 Braga, Portugal (tomas.lopes@inl.int, sourav.bose@inl.int, jr.barbosa@campus.fct.unl.pt, jerome.borme@inl.int, olivier.donzel-gargand@angstrom.uu.se, cc.rocha@campus.fct.unl.pt, rbe.silva@campus.fct.unl.pt, paulo.fernandes@inl.int and pedro.salome@inl.int).

J. M. V. Cunha and P. M. P. Salomé are with Departamento de Física, Universidade de Aveiro, Campus Universitário de Santiago, 3810-193 Aveiro, Portugal.

S. Bose, O. Donzel-Gargand, A. Hultqvist, W. C. Chen and M. Edoff are with Ångström Laboratory, Solid State Electronics, Ångström Solar Center, Uppsala University, SE-751 21 Uppsala, Sweden. (adam.hultqvist@angstrom.uu.se, chen.weichao@angstrom.uu.se, and marika.edoff@angstrom.uu.se).

R. Silva and A. G. Silva are with CEFITEC, Departamento de Física, Faculdade de Ciências e Tecnologia, Universidade Nova de Lisboa, Campus de Caparica, 2829-516 Caparica, Portugal (acs@fct.unl.pt).

P. A. Fernandes is with CIETI, Departamento de Física, Instituto Superior de Engenharia do Porto, Instituto Politécnico do Porto, Rua Dr. António Bernardino de Almeida, 431, 4200-072 Porto, Portugal and also with I3N, Universidade de Aveiro, 3810-193 Aveiro, Portugal.

metals may diffuse and react with the absorber layer considering the growth temperature reached (around 550 ºC) during the standard CIGS processing [17]. Nevertheless, the replacement of Mo by Au has been demonstrated by performing the metal deposition on the absorber after a complex CIGS lift-off process [18]. Despite achieving good results, this method is not suitable for large scale production. Metals, such as tungsten (W) and tantalum (Ta) have been tested and have shown to survive the CIGS growth process, as demonstrated by Orgassa *et al.* [19]. However, they provide significant lower solar cell performance than the standard Mo. Mo has been empirically shown as the material that works the best as rear CIGS contact even with its known optical limitations due to a variety of properties, which include a good electrical contact [20], [21] based on the complex interface between Mo and CIGS with the formation of $MoSe_2$ [21], [22].

In this work, we propose an industrial-friendly and novel alternative for increasing the rear optical reflection. This new, Mo/interlayer/Al_2O_3, rear architecture (shown in Figure 1) brings the following benefits: i) increases the rear optical reflection; ii) passivates the CIGS rear interface with the Al_2O_3 layer; iii) allows for a beneficial electrical contact with CIGS by using the rear Mo layer. Such benefits are possible, since the interlayers are also etched allowing for a direct contact between the CIGS and the Mo while keeping the rest of the surface passivated and with the interlayer dominating the optical behavior. To evaluate this new architecture, we performed an optical simulation of the structures, followed by the fabrication and analysis of resulting solar cells. The optical simulations were performed considering the stack shown in Figure 1. Moreover, the following thicknesses were used: 350 nm for Mo; 20 nm for interlayer; 18 nm for Al_2O_3; 500 nm for CIGS; 50 nm for CdS; 90 nm for i:ZnO; and 350 nm for ZnO:Al. Such optical simulations will give us a better understanding of the optical effects of the materials that will be tested as interlayers in this work, which ultimately will allow us to find the most suitable metal to be used in our structure.

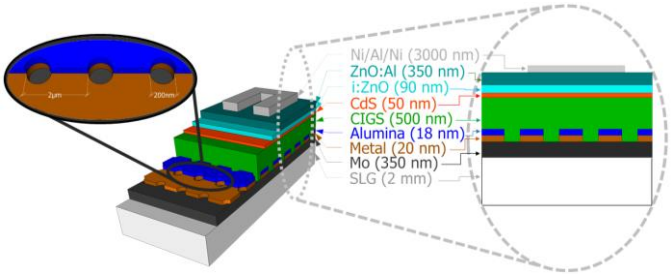

Figure 1 – Schematic representation of the thin film solar cell used here with the inset showing the point contact structure used. Inset representing both pitch size (2 μm) and hole diameter (200 nm), as well as, a 2D picture of the fabricated structure.

II. Experimental

The substrate is soda-lime glass (SLG) and the overall stack fabricated is shown in Figure 1, using the Ångstrom solar cell base line fabrication [23], with the addition of an evaporated 15 nm sodium fluoride (NaF) precursor layer on top of the contact structure just prior to the CIGS deposition. The average thickness of CIGS measured using stylus profilometry is (0.5 ± 0.03) μm with the compositional values of [Cu]/([Ga] + [In]) or CGI = 0.85 ± 0.02 and [Ga]/([Ga] + [In]) or GGI = 0.28 ± 0.01 as measured using X-ray fluorescence. Ungraded (flat profile evaporation rates) CIGS absorbers were used [4], [24]. We fabricated: i) one sample without any passivation or interlayer, further called reference; ii) one sample only with the passivation layer (Al_2O_3); and iii) eight samples with the passivation and a metal interlayer. Each substrate produced 12 solar cells after mechanical scribing with a solar cell area of 0.5 cm^2. Interlayers, namely the metals Au, Ag, Cu, Ta, Ti, Zn, and metal alloys, Ti-W and Al-Si-Cu, with a thickness of 20 nm, were deposited by DC sputtering on the Mo and before the Al_2O_3 layer deposition. The TiW composition is: 97.19 at.% Ti and 2.81 at.% W, while the AlSiCu composition is: 98.34 at.% Al, 1.45 at.% Si and 0.21 at.% Cu. The Al_2O_3 was deposited by RF sputtering to a thickness of 18 nm. A TIMARIS Flexible Target Module (FTM) DC/RF Sputter tool was used for the deposition of the Al_2O_3 and metal alloy layers while the metal layers were deposited using a Kenosistec multi-target UHV sputtering system. For the pattern generation, a Vistec EBPG 5200 e-beam lithography tool was used with an acceleration voltage of 100 kV. Square arrays dots with equivalent diameter approximately 200 nm and pitch size of 2 μm were produced in 12 hours and reactive ion etching was done using SPTS Inductively Coupled Plasma (ICP) tool in the opening of the exposed array. The pattern dimensions were chosen based on our previous results [11], [25]. The details of the fabrication procedure can be found elsewhere [4]. A schematic representation is shown in the inset of Figure 1.

To study the solar cells electrical behavior, illuminated and dark current density against voltage (J-V) at AM1.5 and external quantum efficiency (EQE) measurements were performed in home-built systems.

Optical simulations of the full solar cell stack were conducted using a 3D Finite-Difference Time-Domain (FDTD) numerical method, employing the commercial software, *Lumerical* [26]. To achieve high accuracy while minimizing computational requirements, our optical model was modified as follows: i) the symmetry of the fabricated solar cell stack allowed us to simulate only a quadrant of the solar cell stack, with the use of symmetrical and non-symmetrical boundary conditions (BCs); ii) the mesh size was adapted to our structures; and iii) on the upper boundary condition, a perfectly matched layer was applied and at the lower a metallic BC was used. To corroborate the optical simulation results, a comparison of the optical spectra obtained by the FDTD with analytical formalisms based on the transfer matrix method was conducted. Optical data of the CIGS layer was taken from [27] for CGI=0.3. For the materials Al_2O_3, Au, Ag, Cu and Ti, the optical data was taken from [28], for Ta and Zn the values were taken from [29] and for AlSiCu, it was taken from [30].

The transmission electron microscopy (TEM) lamella preparation was performed using a Ga-based Focused Ion Beam (FIB) from FEI (Helios NanoLab 450S DualBeam) with a low kV final polishing (< 2 kV). The TEM analyses were achieved on either a probe corrected Titan G2 or a probe corrected Titan Themis, both from FEI.

III. Results and Discussion

A. Optical simulations

Optical simulated values for the current density (J_{sc}) and current density losses at the rear contact for each ultrathin device are shown in Table I. Optical simulations for CIGS thickness of 2000 nm and 500 nm are shown in Figure 2 a). Both simulated CIGS layers have a GGI composition of 0.3. These simulations only accounts for optical losses and no electrical losses are modelled. When reducing the CIGS thickness from 2000 nm to 500 nm, it is evident that for wavelength values higher than 700 nm, the ultrathin absorber starts to underperform in comparison with the standard thickness. In this spectral region, a significant lower amount of light is being absorbed in the CIGS. It is worth to point out that the optical simulation considers that all the light absorbed by the CIGS contributes to photocurrent generation, as such, the following losses are not considered by the simulation: electrical losses; inter-elemental diffusion between layers; grain boundaries losses, just to name a few. Accordingly, the standard cell would reach a J_{sc} value of 33.20 mA/cm^2, whereas the ultrathin one would reach a J_{sc} value of 30.55 mA/cm^2. Ultrathin devices have significant optical losses, due to the low value of the light absorption coefficient for wavelength values higher than 600 nm [5], [16], [19], [27]. For the total reflectance of the cell, it only varies significantly of the two thickness for wavelengths higher than 1000 nm. Hence, the difference between a wavelength of 700 nm and of 1000 nm in the amount of light absorbed in the CIGS is compensated by light being absorbed in the Mo layer. In fact, even for a 2000 nm thick CIGS layer according to the optical simulations of our flat and high-Ga/(Ga+In), around 0.17 mA/cm^2 is still absorbed in the Mo layer, in accordance with the literature [19], [31]. The Mo parasitic light absorption is even more severe for the 500 nm thick CIGS sample, with the Mo absorption reaching values of 30 % for a wavelength of 1100 nm. Therefore, an increase of the rear optical reflection could lead to a decrease in optical losses on ultrathin devices. The absorptance of fabricated structures were simulated with the following stack: Mo/interlayer/Al_2O_3/CIGS/CdS/i:ZnO/ZnO:Al, with the results presented in Figure 2 b). All studied metals increase the CIGS light absorption, with Cu, AlSiCu, Au and Ag showing notable results due to their extremely high optical reflection. In Figure 2 c), we represent the amount of light that is absorbed by the Mo and interlayers. Apart from Ti and TiW, all other combinations showed a significant reduction in the parasitic absorption of the rear contact. The introduction of an Al_2O_3 layer already prevents some of the optical losses. The increase of J_{sc} by the insertion of an Al_2O_3 layer in between the CIGS and Mo has been experimentally observed previously [4], [11]. The reduction in parasitic absorption was not observed for Ti and TiW, which might be caused by the 20 nm thick metal layer that already absorbs a significant amount of light. The other interlayers are also 20 nm thick, however for them, the material is not thick enough to show a significant parasitic absorption effect. Figure 2 d) shows the results of the solar cells total optical reflectance simulations for the studied interlayers. We observed that, in comparison with the reference sample, all interlayers improve the cell optical reflection for wavelength values higher than 950 nm. Such simulated results are an indication that an increase in the rear optical reflection will have to be followed by a light trapping strategy [13], [16], [32], [33]. Furthermore, the enhanced rear optical reflection in the infrared region does not contribute only to increased light absorbed in the CIGS layer, but also to an increase in the light exiting the solar cell through the top layer by reflection. The optical simulation was done assuming that the interlayers would remain as they were deposited during the CIGS growth, which is the ideal case. This assumption needs to be experimentally tested as some of these metals may diffuse into CIGS during its growth, and mat react with Se [17], [19], [34]. Other optical effects, such as light scattering due to e.g., grain boundaries and layers roughness can also create differences between the simulations and real results.

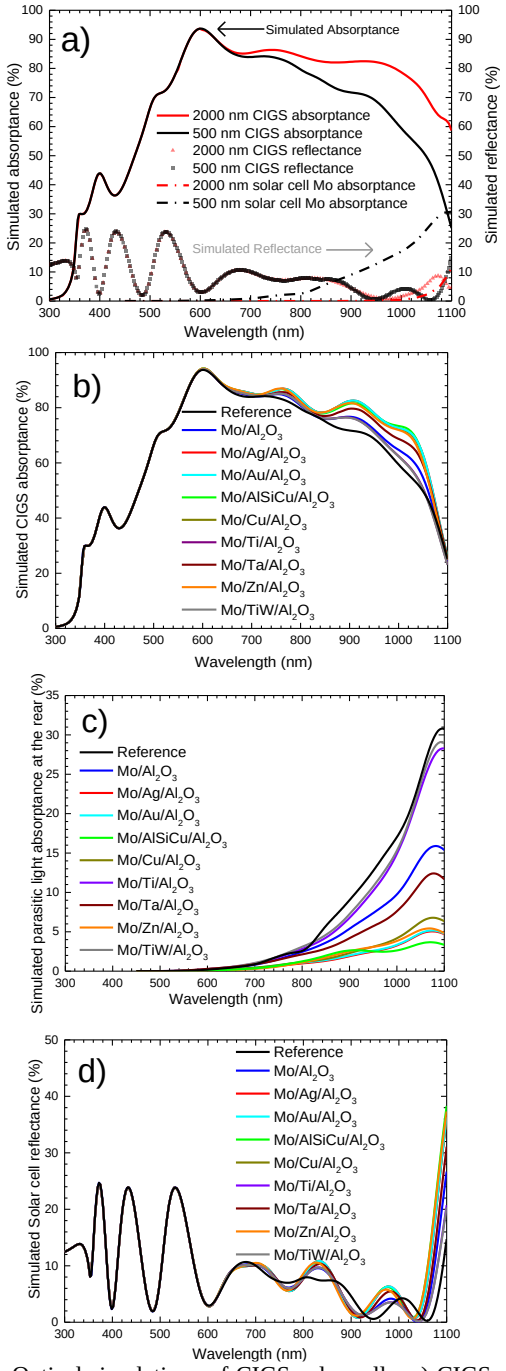

Figure 2 – Optical simulations of CIGS solar cells: a) CIGS and Mo light absorbance and cell reflectance for a 2000 and a 500 nm solar

cell; b) CIGS light absorbance for different interlayers; c) Parasitic light absorption in the Mo and interlayers; d) Total cell reflectance.

TABLE I - SIMULATED J_{SC} FOR ALL THE SOLAR CELLS, AS WELL AS, THE J_{SC} CORRESPONDING TO THE PARASITIC LIGHT ABSORPTION AT THE REAR.

Simulated stack	Color plot	J_{sc} (mA/cm^2)	Parasitic absorption (Mo and interlayer) (mA/cm^2)
Reference		30.55	2.40
Mo/Al_2O_3		31.16	1.49
Mo/Ag/Al_2O_3		32.17	0.50
Mo/Au/Al_2O_3		32.16	0.53
Mo/AlSiCu/Al_2O_3		32.10	0.48
Mo/Cu/Al_2O_3		32.12	0.64
Mo/Ti/Al_2O_3		30.99	2.13
Mo/Ta/Al_2O_3		31.68	1.16
Mo/Zn/Al_2O_3		31.99	0.57
Mo/TiW/Al_2O_3		30.96	2.22

B. Solar cell characterization

Solar cells were fabricated and analyzed in order to compare simulations with real devices measurements. J-V and EQE measurement of the most efficient cells are shown in Figure 3 and Figure 4, respectively. The extracted J-V figures of merit, with average values, standard deviation values and the values of the cell with the highest efficiency cells, are shown in Table II. The reference device has an average efficiency value of 6.2 %, which is expectedly low due to rear interface recombination and incomplete light absorption, characteristic of ultrathin CIGS solar cells and comparable with other works [5], [8], [18], [24], [32], [35], [36]. With the Al_2O_3 passivation layer, an increase in V_{oc} from 535 mV (reference) to 558 mV is observed, which is a good indication of the passivation effect created by the Al_2O_3 layer [4], with mitigation of rear interface recombination. Moreover, an increase in J_{sc} is also observed that can be correlated to the rear optical reflection created by the passivation layer as predicted in the optical simulations. The J_{sc} enhancement of the passivated device over the reference solar cell, 0.61 mA/cm^2 simulated vs 0.40 mA/cm^2 measured, is quite close. The low increase in the measured J_{sc} of the Mo/Al_2O_3 device is clearly affected by the increased standard deviation (1.78 mA/cm^2) in comparison to the one of the reference device, (0.39 mA/cm^2). Such significant difference of the standard deviation can be due to the non-optimized increased processing and manual handling that the passivation requires that may lead to additional problems like impurities, oxidation, effect of humidity, among others. Nonetheless, the increase in V_{oc} and J_{sc} allows for the passivated sample to achieve 1.5 % enhancement on the light to power conversion efficiency values over the reference sample (7.7 % vs 6.2 %). Regarding the J-V plots, the reference sample shows signals of shunting behavior in both light and dark curves. Unpassivated ultrathin solar cells are more likely to have shunts [37]–[40], since pinholes throughout the device have a higher chance of being present from the Mo to the top layers just because the CIGS layer is thinner, mainly when compared with grain size. By applying the Al_2O_3 passivation layer, the shunting problems are effectively suppressed, as most of the area is covered by an insulator. A roll-over behavior is present in the J-V measurement of the passivated sample, as shown in Figure 3 a), which could be related with the lack of sodium (Na) in the CIGS [41], [42]. It is worth to mention that for ultrathin devices the ideal Na quantity, and therefore in this particular case, the NaF precursor thickness, is yet to be optimized. Hence, without such optimization studies, the NaF thickness in this study was kept the same for all the samples. Concerning the devices with the interlayer, with the exception of the TiW device, all other show significant degradation in the electrical performance. As already mentioned, these limitations are likely due to metals diffusion into the CIGS and/or by selenization of the interlayer leading to contact problems as there are small but direct contacts between the interlayer and the CIGS during its growth. The devices with Cu and Au are heavily shunted, as it is shown by the J-V curves and the poor EQE response of the Au sample, as it is presented in Figure 4. Such problem was expected for Cu, as this metal diffuses very easily into the CIGS [43]–[45]. An interesting remark is that the remaining samples, although showing some photo-conductivity, have all different issues and underperform compared even with the reference sample. The Ag and Zn samples show diode-like behavior, nevertheless, the poor electrical performance is attributed to the inter-elemental diffusion and selenization of such metals [46], [47]. In the case of Ag, the light curve shows some shunting behavior while the dark does not. Such behavior is possibly affected by voltage-dependent charge collection (VDCC) [46]. One of the most likely explanation for VDCC is high rear interface recombination in the CIGS, explaining the low V_{oc} and J_{sc} values for the Ag sample [4]. The sample with the Zn interlayer might be suffering from the formation of ZnSe, an n-type compound, which lowers the performance of chalcogenide solar cells when present [47]. The AlSiCu, Ti and Ta samples suffer from current blocking behavior, as it is shown in Figure 3 b). Again, inter-elemental diffusion and selenization is likely to happen, creating compounds that may be acting as a current barrier. These interlayers might selenize and expand due to the formation of the chalcogenide material and physically prevent the CIGS to be in contact with the Mo. Moreover, we noticed that the scribing procedure of Ta and Ti samples was somewhat compromised with cells not fully defined. This fact can lead to interconnections between cells, which could explain, for example, the high J_{sc} figures, the strange FF values, and the odd EQE behavior. The TiW sample had typical good diode dark and illuminated J-V curves without any evident problems, as shown for the other interlayers samples. Moreover, the highest V_{oc} value was achieved by the TiW sample, as well as one of the highest J_{sc} values. Therefore, TiW is a promising rear reflective material with an average efficiency of 9.9 % (best cell with 11.0 %) and all solar cell figures of merit show significant increase both with the reference (3.7% increase) and with the passivated device (2.2 % increase). The simulated J_{sc} value of the TiW sample (30.96 mA/cm^2) was the lowest simulated value among all the interlayers (but higher than the reference one), which means that the major gain in the experimental value of the TiW J_{sc} is likely electrical. Extreme changes in the recombination velocity leads to significant changes in a first

instance in V_{oc} and in a second instance in J_{sc} values as well [6], [9], [11], [48]. At this point, it cannot be discarded that the TiW might help the substrate and sample processing to be optimized in comparison with the other samples, in particular the Al_2O_3 sample, as this could be a simple explanation why this structure performs better than the standard one. More complex explanations for the TiW superior performance may be related with for instance an increased built-in electrical field due to the TiW work function, just to give a specific example. In any case, the enhancement in the J_{sc} as well as the outstanding enhancement in V_{oc} needs to be explored and understood, since these results appear to show that the passivation effect is increased when TiW and Al_2O_3 are used in combination.

TABLE II - J-V FIGURES OF MERIT: AVERAGES; STANDARD DEVIATION VALUES AND THE VALUES FOR THE CELL WITH THE HIGHEST EFFICIENCY IN PARENTHESES.

Sample	V_{OC} (mV)	J_{SC} (mA/cm^2)	FF (%)	Eff (%)
Mo	535 ± 14 (556)	24.28 ± 0.39 (24.81)	47.5 ± 4.6 (53.7)	6.2 ± 0.9 (7.4)
Mo/Al_2O_3	558 ± 23 (583)	24.68 ± 1.78 (26.51)	55.2 ± 4.0 (60.9)	7.7 ± 1.2 (9.4)
Mo/Ag/Al_2O_3	365 ± 13 (378)	15.43 ± 3.02 (19.20)	49.9 ± 2.2 (51.5)	2.8 ± 0.7 (3.7)
Mo/Au/Al_2O_3	191 ± 77 (316)	22.19 ± 1.61 (24.46)	26.1 ± 1.4 (29.6)	1.2 ± 0.6 (2.3)
Mo/AlSiCu/ Al_2O_3	404 ± 66 (553)	0.47 ± 0.11 (0.67)	21.6 ± 1.2 (19.8)	0.0 ± 0.0 (0.0)
Mo/Cu/Al_2O_3	2 ± 1 (4)	1.34 ± 0.30 (1.92)	0.0 ± 0.0 (0.0)	0.0 ± 0.0 (0.0)
Mo/Ti/Al_2O_3	532 ± 15 (544)	28.66 ± 2.57 (30.78)	25.8 ± 1.4 (27.0)	4.0 ± 0.5 (4.5)
Mo/Ta/Al_2O_3	519 ± 41 (579)	16.12 ± 6.73 (24.51)	14.5 ± 2.0 (15.7)	1.2 ± 0.6 (2.2)
Mo/Zn/Al_2O_3	590 ± 8 (597)	23.63 ± 1.59 (23.88)	51.1 ± 2.5 (53.7)	7.1 ± 0.5 (7.7)
Mo/TiW/ Al_2O_3	629 ± 6 (635)	25.25 ± 0.81 (25.80)	61.9 ± 4.5 (67.2)	9.9 ± 1.0 (11.0)

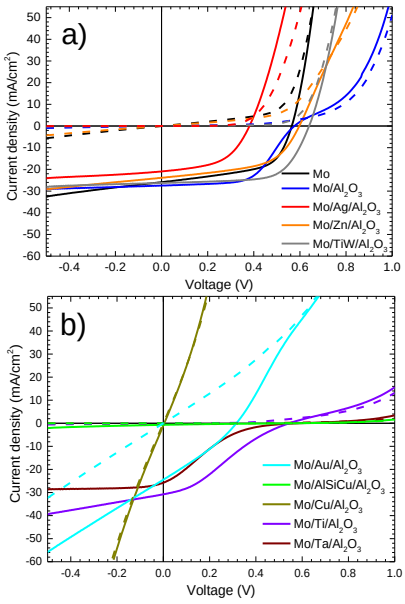

Figure 3 - J-V plots of the highest efficiency devices: a) diode behavior samples and b) samples without diode behavior. Solid lines: Illuminated J-V and dot lines: Dark J-V.

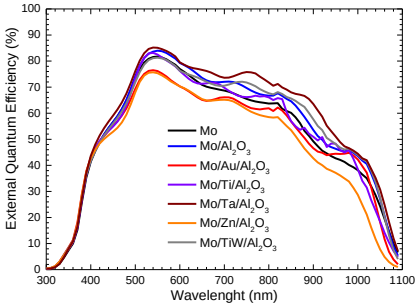

Figure 4 - External quantum efficiency spectra of the highest efficiency devices.

C. *Morphological characterization of the TiW device*

Cleaved samples cannot be decently observed in Scanning Electron Microscopy (SEM) because of the very small dimensions of the interlayers (20 nm) and of the Al_2O_3 (18 nm). We then performed Transmission Electron Microscopy (TEM) analyses in order to obtain high resolution cross-sections of the deposited structures, as shown in Figure 5. Only the TiW sample was analyzed as this was the most interesting sample of the set and FIB+TEM is a very time consuming technique for us to analyze all of the samples that showed degraded performance. Unfortunately we could not find a contact during the extremely complex FIB procedure but the analysis of the interface can, nonetheless, be done. We observe that the Al_2O_3 layer fully covers the interlayer and that no reaction between the TiW and the CIGS is observed. Such fact is in very good agreement with the electrical results, meaning that most of the CIGS surface is in contact with the passivation layer allowing for a reduction of the interface defects. Moreover the TiW is not degrading during the CIGS processing allowing for the expected electrical and optical enhancement of the devices.

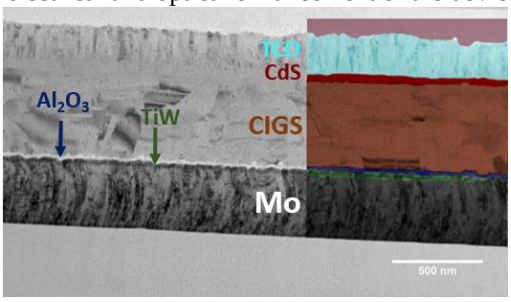

Figure 5 – Bright Field TEM image of the Mo/TiW/Al_2O_3 structure cross-section. The brighter and darker layer in between the CIGS and the Mo are the Al_2O_3 and the TiW, respectively.

IV. CONCLUSIONS

In this work, we present a novel solar cell architecture that comprises of the use of metals/alloys, as interlayers between the Mo rear contact and an Al_2O_3 passivation layer in order to improve rear optical reflection while keeping a passivation effect. Such architecture demonstrates the potential to both passivate the rear contact and to increase the optical reflection. Optical simulations show the importance of improved rear optical reflection as ultrathin CIGS has significant optical losses in the infrared region. By adding a highly reflective layer between the Mo and the Al_2O_3 passivation layer, some of these optical losses for ultrathin devices could be mitigated. Experimentally, the TiW alloy provided solar cells with average light to power conversion efficiency values of 9.9 % (11.0 %

champion cell), which is 2.2% (abs) higher than the solely passivated sample and 3.7 % (abs) higher than the reference sample, by improving all solar cell figure of merit compared with the reference and with the passivation (without the interlayer) devices. This improvement is in agreement with the expected effect of the passivation layer and with the demonstrated optical simulations. TEM cross section measurements showed that both the TiW and the Al_2O_3 layer survive the harsh CIGS processing and that remain conformal over the surface. All other tested metals provided worse results and such fact is attributed to inter-elemental diffusion into the CIGS through the nano-contacts present in the Al_2O_3 layer and/or selenization of the interlayers during the absorber growth. The encountered problems were vastly different and surprisingly even caused problems for cell scribing (Ta, Ti).

In summary, the outstanding improvement in performance by using the novel architecture with the TiW with a champion cell of 11.0 % for 500 nm CIGS absorber thickness, opens the door to further optimization in ultrathin devices and further studies should be focused on improving the fabrication process for large-areas and on understanding in detail the different electrical and optical gains.

REFERENCES

[1] M. A. Green *et al.*, "Solar cell efficiency tables (Version 53)," *Prog. Photovoltaics Res. Appl.*, vol. 27, no. 1, pp. 3–12, Jan. 2019.

[2] "Solar Frontier Achieves World Record Thin-Film Solar Cell Efficiency of 23.35%," 2019. [Online]. Available: http://www.solar-frontier.com/eng/news/2019/0117_press.html. [Accessed: 20-Mar-2019].

[3] V. Fthenakis, "Sustainability of photovoltaics: The case for thin-film solar cells," *Renew. Sustain. Energy Rev.*, vol. 13, no. 9, pp. 2746–2750, Dec. 2009.

[4] P. M. P. Salomé *et al.*, "Passivation of Interfaces in Thin Film Solar Cells: Understanding the Effects of a Nanostructured Rear Point Contact Layer," *Adv. Mater. Interfaces*, vol. 5, no. 2, p. 1701101, Jan. 2018.

[5] N. Naghavi *et al.*, "Ultrathin Cu(In,Ga)Se_2 based solar cells," *Thin Solid Films*, vol. 633, pp. 55–60, Jul. 2017.

[6] B. Vermang, V. Fjällström, J. Pettersson, P. Salomé, and M. Edoff, "Development of rear surface passivated Cu(In,Ga)Se_2 thin film solar cells with nano-sized local rear point contacts," *Sol. Energy Mater. Sol. Cells*, vol. 117, pp. 505–511, Oct. 2013.

[7] M. A. Green, "The Passivated Emitter and Rear Cell (PERC): From conception to mass production," *Sol. Energy Mater. Sol. Cells*, vol. 143, pp. 190–197, Dec. 2015.

[8] B. Vermang *et al.*, "Employing Si solar cell technology to increase efficiency of ultra-thin Cu(In,Ga)Se_2 solar cells," *Prog. Photovoltaics Res. Appl.*, vol. 22, no. 10, pp. 1023–1029, Oct. 2014.

[9] B. Vermang *et al.*, "Introduction of Si PERC Rear Contacting Design to Boost Efficiency of Cu(In,Ga)Se_2 Solar Cells," *IEEE J. Photovoltaics*, vol. 4, no. 6, pp. 1644–1649, Nov. 2014.

[10] J. M. V. Cunha *et al.*, "Insulator Materials for Interface Passivation of Cu(In,Ga)Se_2 Thin Films," *IEEE J. Photovoltaics*, vol. 8, no. 5, pp. 1313–1319, Sep. 2018.

[11] S. Bose *et al.*, "A morphological and electronic study of ultrathin rear passivated Cu(In,Ga)Se_2 solar cells," *Thin Solid Films*, vol. 671, pp. 77–84, Feb. 2019.

[12] M. Schmid, P. Manley, A. Ott, M. Song, and G. Yin, "Nanoparticles for light management in ultrathin chalcopyrite solar cells," *J. Mater. Res.*, vol. 31, no. 21, pp. 3273–3289, Nov. 2016.

[13] G. Yin *et al.*, "Well-Controlled Dielectric Nanomeshes by Colloidal Nanosphere Lithography for Optoelectronic Enhancement of Ultrathin Cu(In,Ga)Se_2 Solar Cells," *ACS Appl. Mater. Interfaces*, vol. 8, no. 46, pp. 31646–31652, Nov. 2016.

[14] S. Suresh *et al.*, "A study to improve light confinement and rear-surface passivation in a thin-Cu(In, Ga)Se_2 solar cell," *Thin Solid Films*, Nov. 2018.

[15] O. Isabella, R. Vismara, D. N. P. Linssen, K. X. Wang, S. Fan, and M. Zeman, "Advanced light trapping scheme in decoupled front and rear textured thin-film silicon solar cells," *Sol. Energy*, vol. 162, pp. 344–356, Mar. 2018.

[16] G. Yin, P. Manley, and M. Schmid, "Light trapping in ultrathin $CuIn_{1-x}Ga_xSe_2$ solar cells by dielectric nanoparticles," *Sol. Energy*, vol. 163, pp. 443–452, Mar. 2018.

[17] R. J. Matson *et al.*, "Metal contacts to $CuInSe_2$," *Sol. Cells*, vol. 11, no. 3, pp. 301–305, Apr. 1984.

[18] Z. J. Li-Kao *et al.*, "Towards ultrathin copper indium gallium diselenide solar cells: proof of concept study by chemical etching and gold back contact engineering," *Prog. Photovoltaics Res. Appl.*, vol. 20, no. 5, pp. 582–587, Aug. 2012.

[19] K. Orgassa, H. W. Schock, and J. H. Werner, "Alternative back contact materials for thin film Cu(In,Ga)Se_2 solar cells," *Thin Solid Films*, vol. 431–432, pp. 387–391, May 2003.

[20] P. M. P. Salomé, J. Malaquias, P. A. Fernandes, and A. F. da Cunha, "Mo bilayer for thin film photovoltaics revisited," *J. Phys. D. Appl. Phys.*, vol. 43, no. 34, p. 345501, Sep. 2010.

[21] T. Wada, N. Kohara, S. Nishiwaki, and T. Negami, "Characterization of the Cu(In,Ga)Se_2/Mo interface in CIGS solar cells," *Thin Solid Films*, vol. 387, no. 1–2, pp. 118–122, May 2001.

[22] L. Assmann, J. C. Bernède, A. Drici, C. Amory, E. Halgand, and M. Morsli, "Study of the Mo thin films and Mo/CIGS interface properties," *Appl. Surf. Sci.*, vol. 246, no. 1–3, pp. 159–166, Jun. 2005.

[23] J. Lindahl *et al.*, "Inline Cu(In,Ga)Se_2 Co-evaporation for High-Efficiency Solar Cells and Modules," *IEEE J. Photovoltaics*, vol. 3, no. 3, pp. 1100–1105, Jul. 2013.

[24] D. Ledinek, P. Salomé, C. Hagglund, U. Zimmermann, and M. Edoff, "Rear Contact Passivation for High Bandgap Cu(In, Ga)Se_2 Solar Cells With a Flat Ga profile," *IEEE J. Photovoltaics*, pp. 1–7, 2018.

[25] S. Bose *et al.*, "Optical Lithography Patterning of SiO_2 Layers for Interface Passivation of Thin Film Solar Cells," *Sol. RRL*, vol. 2, no. 12, p. 1800212, Dec. 2018.

[26] "High-Performance Nanophotonic Simulation Software - Lumerical." [Online]. Available: https://www.lumerical.com/. [Accessed: 15-Mar-2019].

[27] P. D. Paulson, R. W. Birkmire, and W. N. Shafarman, "Optical characterization of $CuIn_{1-x}Ga_xSe_2$ alloy thin films by spectroscopic ellipsometry," *J. Appl. Phys.*, vol. 94, no. 2, pp. 879–888, Jul. 2003.

[28] E. D. Palik, *Handbook of optical constants of solids*. Academic Press, 1998.

[29] W. S. M. Werner, K. Glantschnig, and C. Ambrosch-Draxl, "Optical Constants and Inelastic Electron-Scattering Data for 17 Elemental Metals," *J. Phys. Chem. Ref. Data*, vol. 38, no. 4, pp. 1013–1092, Dec. 2009.

[30] "Angstrom Sun Technologies Inc. | NK Material List." [Online]. Available: http://www.angstec.com/graph/13. [Accessed: 14-Nov-2018].

[31] B. Bissig *et al.*, "Novel back contact reflector for high efficiency and double-graded Cu(In,Ga)Se_2 thin-film solar cells," *Prog. Photovoltaics Res. Appl.*, vol. 26, no. 11, pp. 894–900, Nov. 2018.

[32] C. van Lare, G. Yin, A. Polman, and M. Schmid, "Light Coupling and Trapping in Ultrathin Cu(In,Ga)Se_2 Solar Cells Using Dielectric Scattering Patterns," *ACS Nano*, vol. 9, no. 10, pp. 9603–9613, Oct. 2015.

[33] G. Yin *et al.*, "Integration of plasmonic Ag nanoparticles as a back reflector in ultra-thin Cu(In,Ga)Se_2 solar cells," *Appl. Surf. Sci.*, vol. 355, pp. 800–804, Nov. 2015.

[34] E. Moons, T. Engelhard, and D. Cahen, "Ohmic contacts to p-$CuInSe_2$ crystals," *J. Electron. Mater.*, vol. 22, no. 3, pp. 275–280, Mar. 1993.

[35] R. Kotipalli *et al.*, "Addressing the impact of rear surface passivation mechanisms on ultra-thin Cu(In,Ga)Se_2 solar cell performances using SCAPS 1-D model," *Sol. Energy*, vol. 157, pp. 603–613, Nov. 2017.

[36] E. Jarzembowski, B. Fuhrmann, H. Leipner, W. Fränzel, and R. Scheer, "Ultrathin Cu(In,Ga)Se_2 solar cells with point-like back contact in experiment and simulation," *Thin Solid Films*, vol. 633, pp. 61–65, Jul. 2017.

[37] A. Duchatelet, E. Letty, S. Jaime-Ferrer, P.-P. Grand, F. Mollica, and N. Naghavi, "The impact of reducing the thickness of electrodeposited stacked Cu/In/Ga layers on the performance of CIGS solar cells," *Sol. Energy Mater. Sol. Cells*, vol. 162, pp. 114–

119, Apr. 2017.
[38] T. Negami, S. Nishiwaki, Y. Hashimoto, N. Kohara, and T. Wada, "Effect of the absorber thickness on performance of Cu(In,Ga)Se_2 solar cells," *Proc. 2nd WCPEC, Vienna*, pp. 1181–1184, 1998.
[39] W. N. Sharaman, R. W. Birkmire, S. Marsillac, M. Marudachalam, N. Orbey, and T. W. F. Russell, "Effect of reduced deposition temperature, time, and thickness on Cu(InGa)Se_2 films and devices," in *Conference Record of the Twenty Sixth IEEE Photovoltaic Specialists Conference*, 1997, pp. 331–334.
[40] O. Lundberg, M. Bodegård, J. Malmström, and L. Stolt, "Influence of the Cu(In,Ga)Se_2 thickness and Ga grading on solar cell performance," *Prog. Photovoltaics Res. Appl.*, vol. 11, no. 2, pp. 77–88, Mar. 2003.
[41] P. M. P. Salomé *et al.*, "Cu(In,Ga)Se_2 Solar Cells With Varying Na Content Prepared on Nominally Alkali-Free Glass Substrates," *IEEE J. Photovoltaics*, vol. 3, no. 2, pp. 852–858, Apr. 2013.
[42] R. Caballero *et al.*, "Influence of Na on Cu(In,Ga)Se_2 solar cells grown on polyimide substrates at low temperature: Impact on the Cu(In,Ga)Se_2/Mo interface," *Appl. Phys. Lett.*, vol. 96, no. 9, p. 092104, Mar. 2010.
[43] K. Gartsman *et al.*, "Direct evidence for diffusion and electromigration of Cu in $CuInSe_2$," *J. Appl. Phys.*, vol. 82, no. 9, p. 4282, Aug. 1998.
[44] J.-F. Guillemoles, L. Kronik, D. Cahen, U. Rau, A. Jasenek, and H.-W. Schock, "Stability Issues of Cu(In,Ga)Se_2-Based Solar Cells," *J. Phys. Chem. B*, vol. 104, no. 20, pp. 4849–4862, May 2000.
[45] U. Rau and M. Schmidt, "Electronic properties of ZnO/CdS/Cu(In,Ga)Se_2 solar cells — aspects of heterojunction formation," *Thin Solid Films*, vol. 387, no. 1–2, pp. 141–146, May 2001.
[46] R. Scheer and H.-W. Schock, *Chalcogenide Photovoltaics*. Weinheim, Germany: Wiley-VCH Verlag GmbH & Co. KGaA, 2011.
[47] J. Timo Wätjen, J. Engman, M. Edoff, and C. Platzer-Björkman, "Direct evidence of current blocking by ZnSe in $Cu_2ZnSnSe_4$ solar cells," *Appl. Phys. Lett.*, vol. 100, no. 17, p. 173510, Apr. 2012.
[48] N. Touafek and R. Mahamdi, "Back Surface Recombination Effect on the Ultra-Thin CIGS Solar Cells by SCAPS," *Int. J. Renew. Energy Res.*, vol. 4, no. 4, p. 958, 2014.